ISSN 0020-1685, Inorganic Materials, 2007, Vol. 43, No. 8, pp. 834–844. © Pleiades Publishing, Inc., 2007.
Original Russian Text © G.Yu. Yurkov, A.S. Fionov, Yu.A. Koksharov, V.V. Kolesov, S.P. Gubin, 2007, published in Neorganicheskie Materialy, 2007, Vol. 43, No. 8, pp. 936–947.

Electrical and Magnetic Properties of Nanomaterials Containing Iron or Cobalt Nanoparticles

G. Yu. Yurkov[a], A. S. Fionov[b], Yu. A. Koksharov[c], V. V. Kolesov[b], and S. P. Gubin[a, d]

[a] *Kurnakov Institute of General and Inorganic Chemistry, Russian Academy of Sciences,*
Leninskii pr. 31, Moscow, 119991 Russia
[b] *Institute of Radio Engineering and Electronics, Russian Academy of Sciences, Mokhovaya ul. 11, Moscow, 125009 Russia*
[c] *Moscow State University, Vorob'evy gory 1, Moscow, 119899 Russia*
[d] *Lomonosov State Academy of Fine Chemical Technology, pr. Vernadskogo 86, Moscow, 117571 Russia*
e-mail: gy-yurkov@mail.ru

Received December 25, 2006

Abstract—We have prepared nanocomposites consisting of narrowly sized metal-containing nanoparticles embedded in a polyethylene matrix and have established conditions for the fabrication of thick films and bulk materials from the synthesized polymer powders. Dielectric permittivity and resistivity measurements demonstrate that the electrical properties of the nanocomposites depend significantly on the nanoparticle size and content. The microwave absorption and permittivity of the materials are shown to vary little in a broad frequency range. The magnetization (including the remanent one) of the cobalt-containing nanomaterials is higher than that of the iron-containing samples.

DOI: 10.1134/S0020168507080055

INTRODUCTION

The study of metal-containing nanoparticles, including those stabilized in polymer matrices, is stimulated by the ever increasing interest in nanotechnology in many areas of chemistry, physics, and materials research [1–6]. The possibility of creating materials that combine properties of polymers and metals, and approaches to tailoring their properties via compositional control have long been discussed in the literature [7, 8]. In this area of research, several stages can be distinguished. First, the most attention was paid to the development of convenient and reproducible processes for the synthesis of metal-containing nanoparticles, their optimization, and amenability to commercial-scale production. Later efforts were focused on effective strategies for stabilizing metal nanoparticles.

It is well known that most materials based on metal-containing nanoparticles are thermodynamically unstable [9]. They can be stabilized using a variety of polymers, e.g., polyethylene [3, 10], polypropylene [3, 11], poly(tetrafluoroethylene) [12, 13], and others [14]. These polymers offer relatively high thermal stability, unique rheological properties, and high dielectric strength. In addition, they are chemically inert and have favorable processing properties, suitable for the fabrication of complex-shaped and large parts. Also important is that there are mature methods for the synthesis of these polymers. As a rule, polymeric materials are good dielectrics with stable physical and chemical properties [15].

Owing to their chemical stability, polymers can be employed under severe conditions but are used primarily as insulators [16].

Note that the mechanical properties of polymers can be tuned using a variety of inorganic fillers [17], which were reported to influence not only the mechanical and thermomechanical properties of polymers [15, 18] but also their electrical characteristics [19–21].

Composites produced by modifying polymer dielectrics with carbon nanotubes [22–24] or metal-containing fillers [16, 21, 25–27] have higher electrical conductivity in comparison with the parent polymer matrix. As shown in the above-mentioned studies, the electrical properties of composites depend on the composition, shape, size, and concentration of filler particles. It is also believed that varying the concentration of nanoparticles in polymers, one can control the electrical properties of the resultant nanocomposites [28, 29].

Note that the above properties depend directly on the concentration, shape, and surface activity of filler particles [30, 31]. Nanometer-sized fillers, particularly nanoparticles, are the most attractive for the fabrication of metal-containing polymer-matrix nanocomposites because they possess a number of unique characteristics missing in bulk materials [31–35].

The study of polymer-matrix nanocomposites is of great importance because such nanosystems offer a unique combination of chemical, physical, mechanical, and processing properties: increased thermal and electrical conductivity, high magnetic susceptibility, and the ability to absorb ionizing radiation.

Metal-containing polymeric materials have been the subject of intense studies because they have considerable potential for many technological applications. Metal–polymer composites can be prepared by a variety of methods: exposure of polymer films to metal vapor, chemical reactions of metal salts in polymer solutions followed by the recovery of the polymer, polymerization of various metal-containing monomeric systems, and others.

Loading polymers with inorganic fillers offers the possibility of creating materials that combine the properties of the filler and matrix [3, 7, 13–16, 35–38].

The polymer best suited to the application area in question is high-pressure polyethylene because it is comparatively inexpensive, and there is mature technology for its production. Another important advantage of polyethylene is that it can easily be mixed with both organic and inorganic fillers [1, 3, 7, 13–16, 21]. Moreover, polyethylene is a thermoplastic polymer, which enables the fabrication of complex-shaped and large parts under mild conditions. Owing to these advantageous properties, polyethylene is widely used in electrical engineering.

The use of such composites as distributed nonlinear components in microwave engineering (to fill waveguide lines and cavities, to produce thin coatings and electromagnetic shields, etc.) is expected to culminate in a diversity of novel devices for electromagnetic signal conversion and stealth applications.

Polyethylene, in particular, high-molecular polyethylene, is being used increasingly as a key component of prosthetic materials. In addition, the high electric strength and resistivity of polyethylene make it an attractive basic component of diverse insulating materials.

The above highlights that the development of effective approaches for the fabrication of polyethylene-matrix composites is a critical issue in composite materials research.

In this paper, we report the synthesis and characterization of nanocomposites in which high-pressure polyethylene is used as a nanoparticle-stabilizing matrix, and the filler consists of iron- or cobalt-containing nanoparticles of controlled size and composition.

EXPERIMENTAL

Samples consisting of iron- and cobalt-containing nanoparticles stabilized in a polyethylene matrix were prepared through thermal decomposition of metal-containing precursors in a high-temperature polyethylene–oil solution [3, 7, 35] at 270–300°C. The metal-containing precursors used in this study were iron(III) formate, $Fe(HCOO)_3 \cdot 2H_2O$; iron pentacarbonyl, $Fe(CO)_5$; iron(II) oxalate, $FeC_2O_4 \cdot 2H_2O$; and cobalt acetate, $Co(CH_3COO)_2 \cdot 4H_2O$. An appropriate amount of a metal-containing precursor was added to a vigorously stirred high-temperature solution of high-pressure polyethylene. The reactor was filled with argon in order to create an inert atmosphere and effectively remove gaseous reaction products. After washing with benzene in a Sohxlet apparatus in order to remove the oil, the sample was vacuum-dried and then stored in air. The resultant materials had the form of gray and black powders

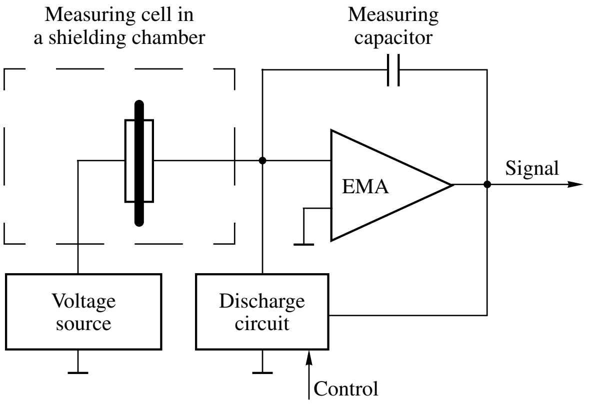

Fig. 1. Schematic of resistivity measurements.

The size of the metal-containing nanoparticles stabilized in a polyethylene matrix was determined by transmission electron microscopy (TEM) on a JEOL JEM-100B (accelerating voltage, 75 kV). To this end, the material was sonicated in ethanol, and the dispersion was applied to a copper grid coated with poly(vinyl formal) and then carbon.

X-ray diffraction (XRD) patterns of powders and compacts were collected on a DRON-3 diffractometer (CuK_α radiation, λ = 1.54056 Å, pyrolytic graphite monochromator, continuous scan rate of 2°/min). Densities were determined by hydrostatic weighing on an all-purpose damped balance with a 5-mg sensitivity. The density of ethanol was taken to be 0.79443 g/cm^3, and that of air, 0.00167 g/cm^3.

Resistivity was measured by a V7E-42 electrometer voltmeter, which ensured direct current measurements in the range 10^{-15} to 0.1 A and resistance measurements from 1 to 10^{18} Ω. At low currents (below 10^{-9} A) and high resistances (above 10^{10} Ω), the measurement accuracy was within 1.5–25.0 and 5.0–50.0%, respectively. In measurements of the current through the sample, the voltage source used was a P320 programmed calibrator, which provided constant voltages in the range 10 μV to 1 kV. The uncertainty in voltage setting was within 0.01%. To eliminate electrostatic noise and electromagnetic interferences, the measuring cell was mounted in a shielding chamber (Fig. 1). The resistance of the sample was measured 1 min after the voltage had been applied for 10 min at 1-min intervals.

At frequencies of 1 kHz and 1 MHz, dielectric permittivity was measured using an E7-8 LCR bridge and E7-12 digital LCR meter, respectively. The E7-8 is

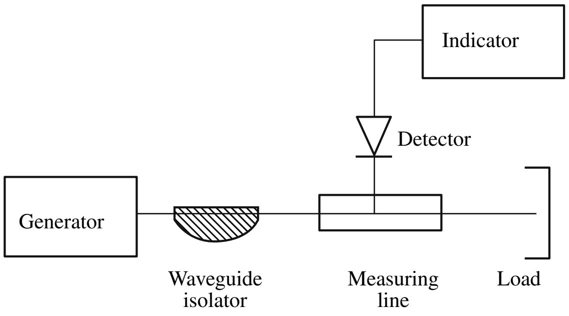

Fig. 2. Block diagram of the measuring system.

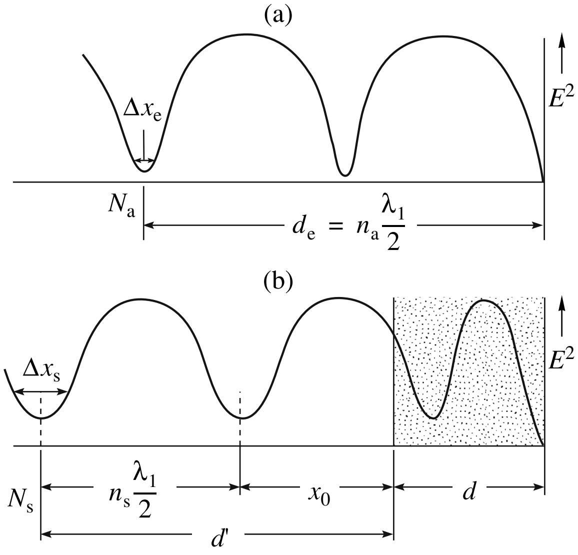

Fig. 3. Standing wave pattern in a short-circuited waveguide: (a) empty, (b) with a sample.

intended for measurements at 1 kHz and ensures capacity measurements in the range 0.01 pF to 100 μF. At typical capacities of the measuring cell, its uncertainty is 3 to 100 pF (within 0.3%). The E7-12 (1-MHz working frequency) ensures capacity measurements in the range 0.001 pF to 100 nF. At typical capacities of the measuring cell, its uncertainty is 3 to 100 pF (within 0.4%).

The dielectric permittivity and absorption of the samples in the frequency range 17.44–53.57 GHz were measured by the short-circuited line method. The block diagram of the measuring system is shown in Fig. 2.

The general principle of dielectric permittivity determination by the short-circuited line method is to measure the voltage standing-wave ratio and the position of the standing wave minimum in an empty short-circuited waveguide and after introducing the material to be studied (Fig. 3) [39, 40].

In our measurements, we used microwave devices operating with a rectangular waveguide: G4-156 generator with an R1-12A measuring line (frequency range 17.44–25.95 GHz, 11 × 5.5 mm waveguide cross section), G4-155 generator with an R1-13A measuring line (frequency range 25.95–37.5 GHz, 7.2 × 3.4 mm waveguide cross section), G4-141 generator with an R1-39 measuring line (frequency range 37.5–53.57 GHz, 5.2 × 2.6 mm waveguide cross section), and Unipan Type 237 selective nanovoltmeter as an indicator. Its output was fed to a V7-38 digital voltmeter.

We used internal square-wave modulation of the generator signal with a repetition rate of 1 kHz. The measuring cell had the form of a waveguide segment, with the sample mounted in its cross section. Under the conditions of this study, the uncertainty in generator frequency setting was within 1.5%, the maximum rated output power of the generators was at least 5 mW, the 15-min instability of the output power was 0.15 dB, and the output voltage standing-wave ratio was within 4. The intrinsic voltage standing-wave ratio of the measuring lines was no greater than 1.03, the probe position was indicated with an uncertainty within 0.05 mm in the entire range of probe displacements, the microwave losses in the line were within 0.3 dB, and the voltage standing-wave ratio of the movable short-circuited load was at least 50. The selective voltmeter ensured ac voltage measurements in the range 1 μV to 100 mV. In the working frequency range, the uncertainty in voltage measurements was within 6% at a 25-dB selectivity.

As a control sample in resistivity, dielectric permittivity, and microwave absorption measurements, we used unloaded high-pressure polyethylene, which went through all of the synthesis and sample preparation steps.

Electron magnetic resonance (EMR) spectra were taken on a Varian E-4 spectrometer at *X*-band (~9.1 GHz), using a Varian E257 variable-temperature attachment. The signal was characterized by its peak-to-peak width ΔH_{pp}, peak-to-peak height A_{pp}, and intensity $I \approx A_{pp}(\Delta H_{pp})^2$.

The size of the synthesized iron- and cobalt-containing nanoparticles was determined by TEM, and their composition was inferred from XRD data.

RESULTS AND DISCUSSION

Figure 4 shows TEM micrographs and XRD patterns of the synthesized nanomaterials.

Characteristically, the XRD patterns of our samples show strong reflections from the stabilizing matrix. The diffraction peaks from the metal-containing component are weaker and broader (for the convenience of interpretation, these peaks are shown on an expanded scale, while the peaks from the polymer matrix are omitted).

According to XRD data, samples 1 and 2, synthesized from $Fe(CO)_5$ (Figs. 4b, 4c), contain nanoparticles with a core–shell structure, as in earlier studies [41–43]. Samples 1 and 2 differ in the concentration of iron-containing nanoparticles in the high-pressure

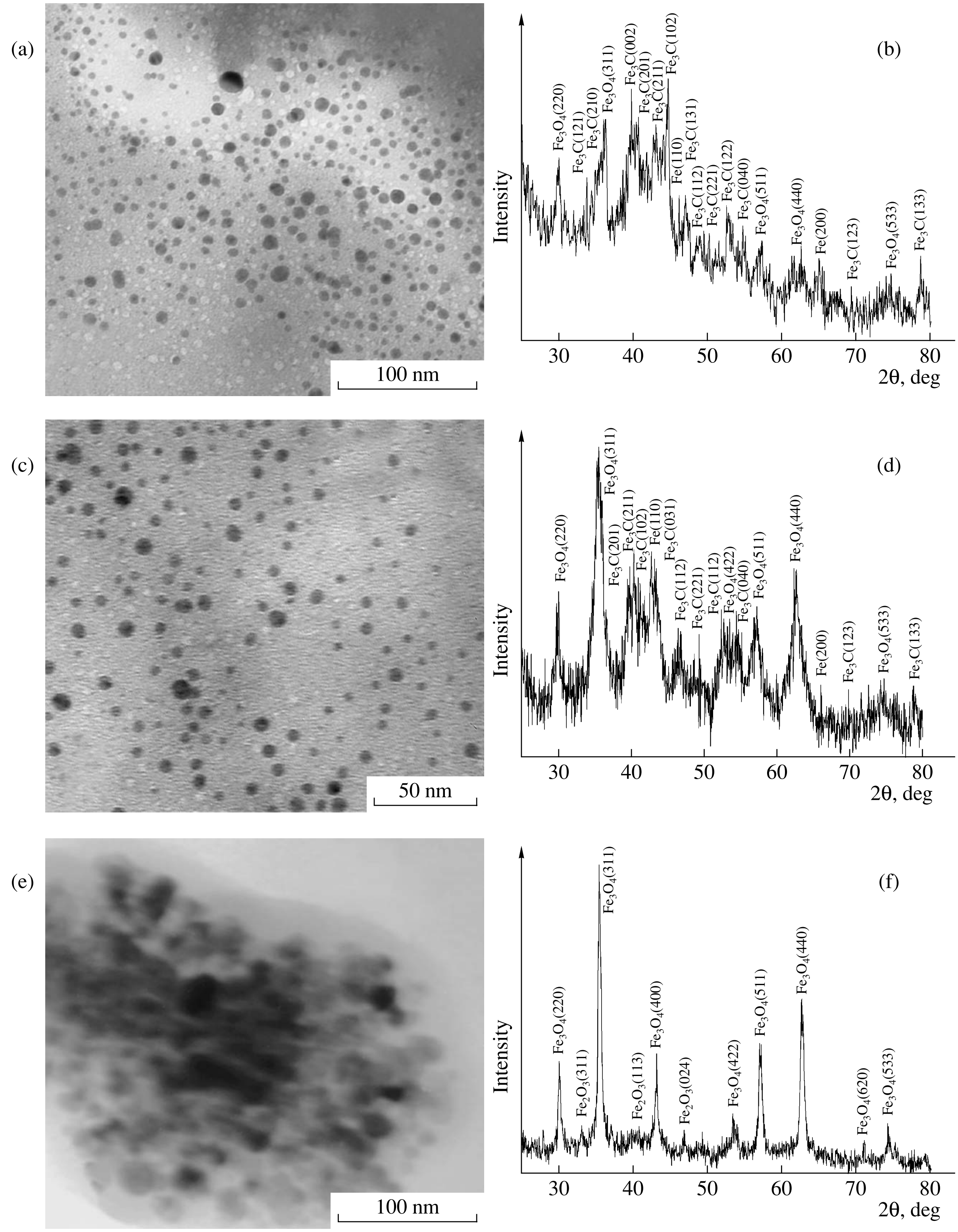

Fig. 4. (a, c, e, g, i) TEM micrographs and (b, d, f, h, j) XRD patterns of the nanocomposites studied: (a–h) iron-containing nanoparticles synthesized from (a–d) iron pentacarbonyl, (e, f) iron(III) formate, and (g, h) iron(II) oxalate; (i, j) cobalt-containing nanoparticles synthesized from cobalt(II) acetate. The composition of the nanoparticles was determined using ICDD PDF 1999 data.

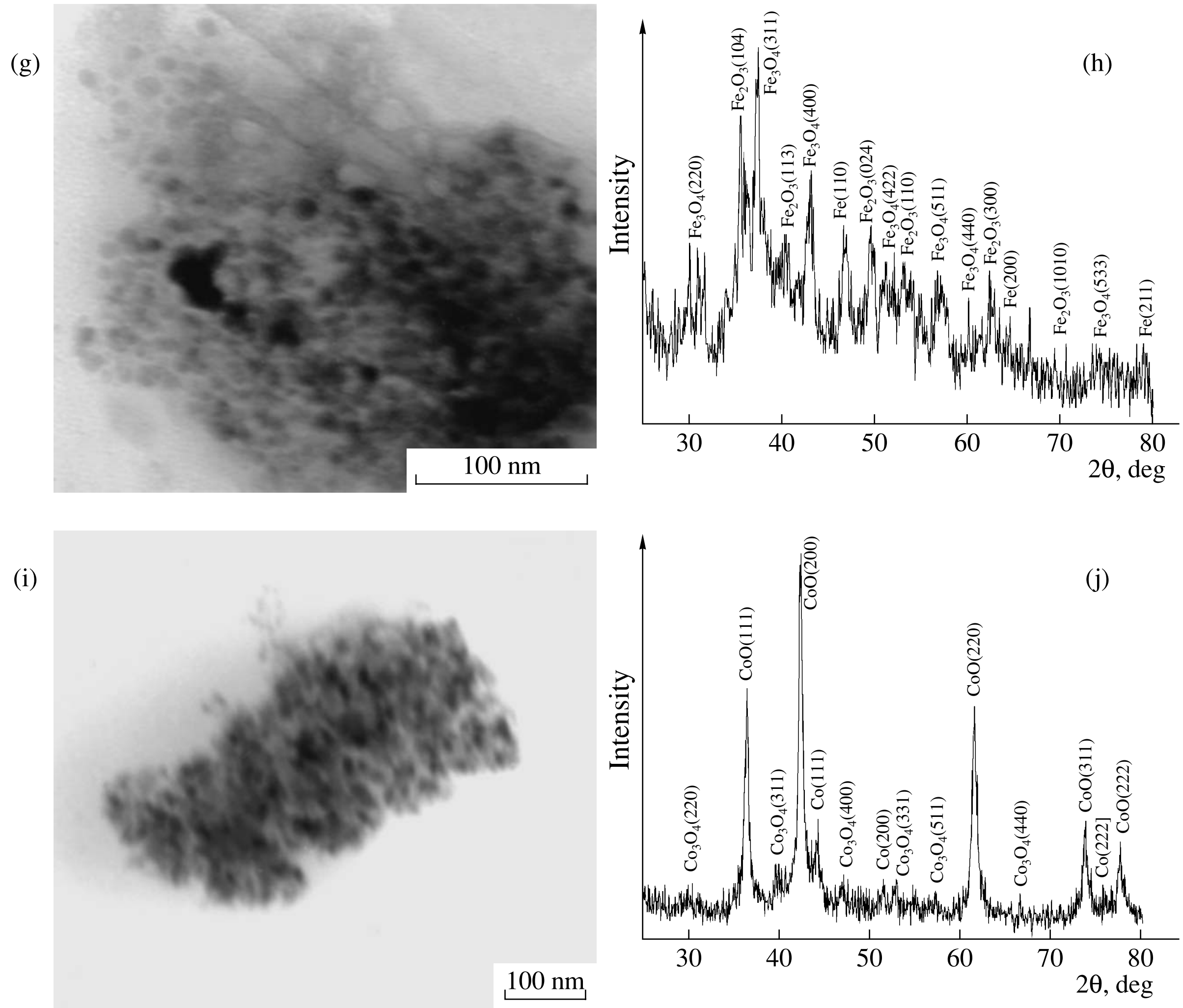

Fig. 4. (Contd.)

polyethylene matrix. The XRD pattern of sample 1 (Fig. 4b) shows weak reflections attributable to Fe_3O_4 (JCPDS 85-1436), Fe_3C (JCPDS 85-1317), and Fe (JCPDS 85-1410). The reflections present in the XRD pattern of sample 2 (Fig. 4d) correspond to Fe_3O_4 (JCPDS 85-1436), Fe_3C (JCPDS 85-1317), and ε-Fe (JCPDS 34-0529). Unfortunately, the major metal-containing component of sample 1 cannot be identified from XRD data. The relative intensities of the reflections from sample 2 suggest that the major iron-containing component of this material is Fe_3O_4. The average size of the iron-containing nanoparticles in samples 1 and 2 is 4.9 and 5.1 nm, respectively, as determined by TEM (Figs. 4a, 4c).

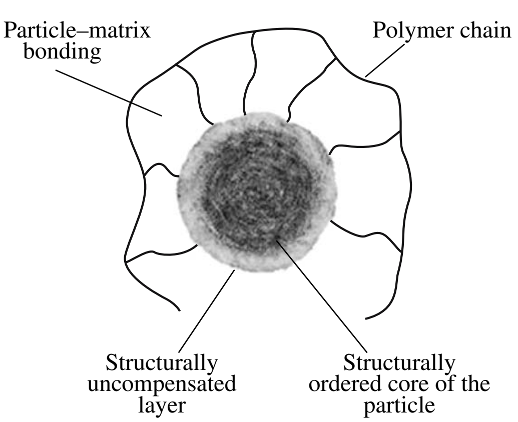

Fig. 5. General model for the structure of the synthesized nanoparticles.

The XRD pattern of sample 3 (Fig. 4f), prepared from iron(III) formate, $Fe(HCOO)_3$, shows reflections characteristic of Fe_2O_3 (JCPDS 86-0550) and Fe_3O_4 (JCPDS 85-1436). XRD intensities indicate that major component of this sample is Fe_3O_4. The average nanoparticle size in sample 3 is 11.5 nm, as determined by TEM (Fig. 4e).

Table 1. Densities of nanocomposites

Material	wt % Fe	ρ_{meas}, g/cm^3	ρ_{calc}, g/cm^3	Volume coefficient
Polyethylene	0	0.94	0.940	1.000
Sample 1	5	0.96	1.006	1.048
Sample 2	10	0.99	1.083	1.094
Sample 3	20	1.23	1.302	1.059

Table 2. Resistivity ρ_V of nanocomposites

Material	wt % nanoparticles	ρ_V, Ω m		
		10 V	100 V	1000 V
Polyethylene	0		$4.9 \times 10^{14} \pm 25\%$	$3.9 \times 10^{14} \pm 5\%$
Sample 1	5	$1.4 \times 10^{14} \pm 50\%$	$1.2 \times 10^{14} \pm 25\%$	$0.9 \times 10^{14} \pm 5\%$
Sample 2	10	$5.5 \times 10^{13} \pm 25\%$	$5.5 \times 10^{13} \pm 10\%$	$4.25 \times 10^{13} \pm 5\%$
Sample 3	20	$4.5 \times 10^{12} \pm 25\%$	$3.0 \times 10^{12} \pm 10\%$	$1.0 \times 10^{11} \pm 5\%$
Sample 4	20	$9.5 \times 10^{13} \pm 25\%$	$5.1 \times 10^{13} \pm 10\%$	$1.5 \times 10^{13} \pm 5\%$
Sample 5	20	$2.8 \times 10^{13} \pm 25\%$	$1.6 \times 10^{13} \pm 10\%$	$5.5 \times 10^{12} \pm 5\%$

The XRD data for sample 4 (Fig. 4h), synthesized through thermal decomposition of iron(II) oxalate, $FeC_2O_4 \cdot 2H_2O$, indicate the presence of Fe_3O_4 (JCPDS 85-1436), Fe_2O_3 (JCPDS 86-0550), and Fe (JCPDS 85-1410). The major component of sample 4 is probably Fe_3O_4; the average nanoparticle size inferred from TEM data is 2.4 nm (Fig. 4g).

The XRD pattern of sample 5 (Fig. 4j), prepared through thermal decomposition of cobalt(II) acetate, shows strong reflections at $2\theta = 36.5°, 42.35°, 61.55°, 73.8°$, and $77.6°$, attributable to CoO (JCPDS 78-0431). There are also a number of weaker reflections attributable to metallic Co (JCPDS 15-0806) and Co_3O_4 (JCPDS 78-1969). In sample 6, the average size of cobalt-containing nanoparticles is 8.3 nm (Fig. 4i), and the major component is CoO, as inferred from XRD intensities. In an earlier study [43], nanoparticles with a similar composition were stabilized on the surface of poly(tetrafluoroethylene) microgranules.

Characteristically, the XRD patterns of nanoparticles stabilized in polymer matrices show a small number of reflections, which are broadened and occasion-

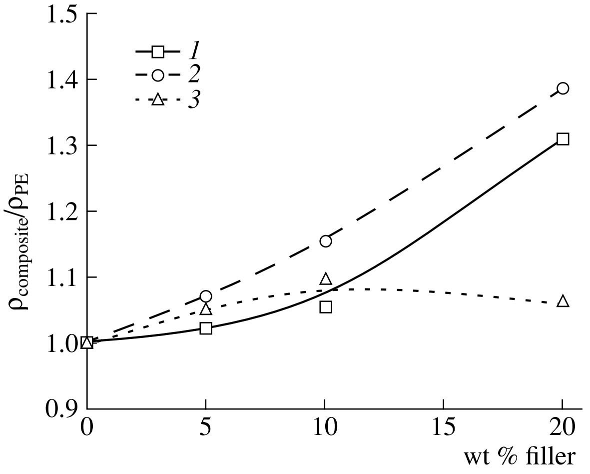

Fig. 6. Reduced density $\rho_{composite}/\rho_{PE}$ as a function of filler content for polyethylene-matrix composites: (*1*) experiment, (*2*) calculation, (*3*) volume coefficient.

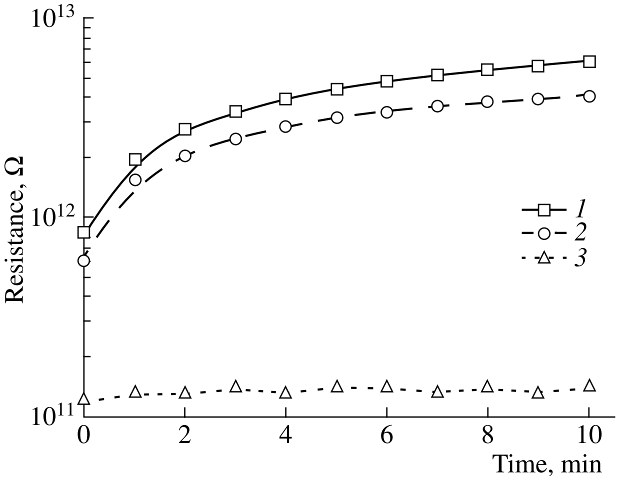

Fig. 7. Resistance of sample 3 as a function of time at an applied voltage of (*1*) 10, (*2*) 100, and (*3*) 1000 V.

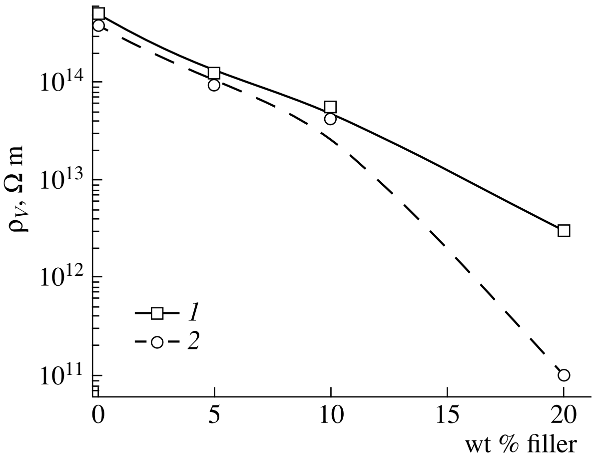

Fig. 8. Resistivity as a function of filler content for samples 1–3 at an applied voltage of (*1*) 100 and (*2*) 1000 V.

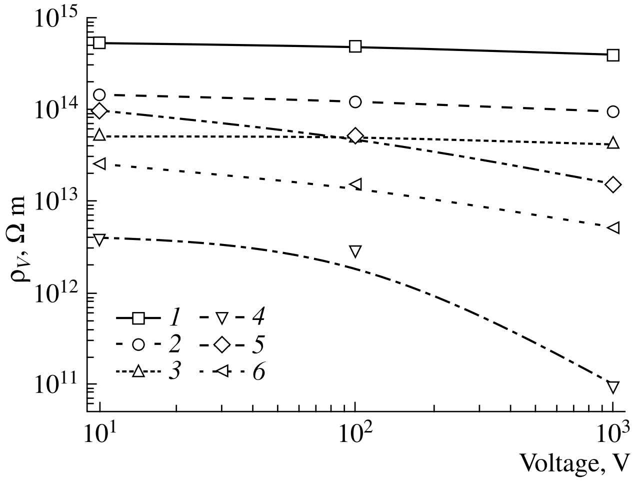

Fig. 9. Resistivity as a function of applied voltage for (*1*) PE and samples (*2*) 1, (*3*) 2, (*4*) 3, (*5*) 4, and (*6*) 5.

ally overlap. Unfortunately, this prevented us from unambiguously determining the composition of the nanoparticles and the exact phase composition of the samples from XRD data. Nevertheless, based on the general trends in the compositions of the synthesized metal-containing nanoparticles, we developed a model of a nanoparticle stabilized in a polymer matrix (Fig. 5), which is consistent with earlier results on the composition of nanoparticles stabilized both in the interior of polymers [12, 35, 41] and on the surface of microgranules [42–44].

The densities of our samples (determined by hydrostatic weighing and calculated) are listed in Table 1. Figure 6 plots the density versus filler content. The volume coefficient in Table 1 is introduced to match the measured densities of the samples to the calculated ones and represents the relative expansion of the polymer matrix upon the introduction of metal-containing nanoparticles. The increase in volume is, most likely, due to an increase in amorphous content and the formation of nanopores in the polyethylene matrix.

The resistivity data for the polymer-matrix composites are presented in Table 2. The plots of sample resistance versus time, filler content, and applied voltage for our materials are displayed in Figs. 7–9.

The permittivity data are presented in Table 3 and Figs. 10 and 11.

The observed magnitudes and time dependences of resistivity lead us to the following conclusion: the electrical transport in the nanocomposites follows the same mechanisms as in unloaded polyethylene (ionic conduction, dipole polarization, displacement polarization, electrical cleaning, electron injection through the electrode–sample interface). The resistivity and dielectric permittivity of the unloaded polyethylene differ from standard values (10^{16} to 10^{18} Ω m and 2.2–2.3, respectively), which is attributable to contamination during processing.

The resistivity of the samples containing 5 and 10 wt % filler (samples 1 and 2), as well as that of unloaded polyethylene, is a weak function of applied voltage and decreases linearly with increasing nanoparticle content over the entire voltage range studied. At a nanoparticle content of 20 wt %, the resistivity is a stronger function of applied voltage: raising the voltage from 100 to 1000 V reduces the resistivity of samples 4 and 5 by a factor of

Table 3. Relative dielectric permittivity of nanocomposites

Material	wt % nanoparticles	ε		Average particle size, nm (TEM data)
		1 kHz	1 MHz	
Polyethylene	0	2.94	2.70	–
Sample 1	5	2.98	2.69	4.9
Sample 2	10	3.63	3.32	5.1
Sample 3	20	4.52	3.56	11.5
Sample 4	20	3.67	3.37	2.4
Sample 5	20	3.96	3.01	8.3

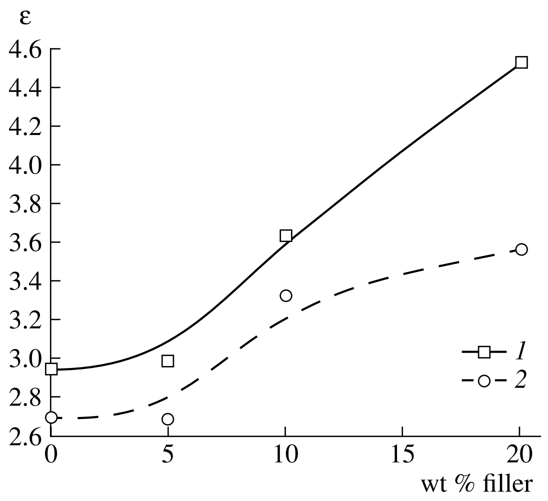

Fig. 10. Low-frequency dielectric permittivity as a function of filler content for samples 1–3: (*1*) 1 kHz, (*2*) 1 MHz.

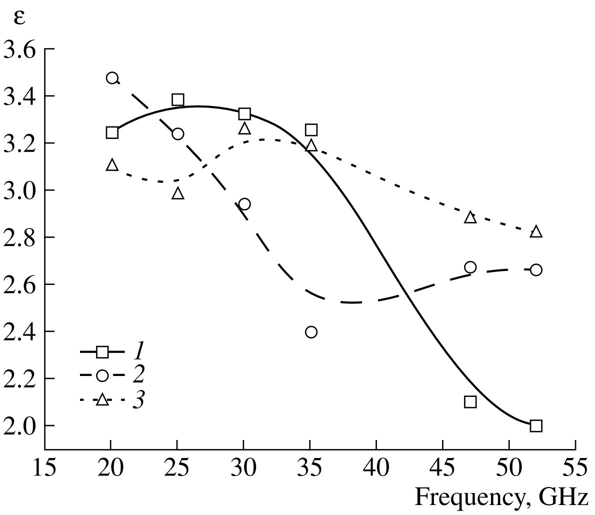

Fig. 11. Microwave dielectric permittivity as a function of frequency: (*1–3*) samples 1–3, respectively.

3 and that of sample 3 by more than one order of magnitude.

The reduction in resistivity upon the introduction of nanoparticles into polyethylene may be due to changes in its structure, such as an increase in amorphous content and porosity, which raise its molecular mobility and reduce the dissociation energy of the ions in the polymer.

An additional contribution to the electrical conductivity of the nanocomposites may come from polarization effects associated with the polarizability of the nanoparticles: macrodisplacement (on the length scale of the sample) and microdisplacement (within local regions) polarization and slowly developing dipole polarization.

The composition and size of the nanoparticles have a complex effect on the electrical conductivity of the loaded high-pressure polyethylene, which is well illustrated by the lower resistivity of sample 3 at a voltage of 1000 V in comparison with that of samples 4 and 5.

The systematic increase in permittivity with increasing filler content is due to the contribution from the polarization of the metal-containing nanoparticles, whose polarizability is higher than that of the matrix owing to the higher mobility of electron shells. As a result, the permittivity increases with filler content.

Samples 3 and 4, though identical in the concentration of iron-containing nanoparticles, differ in permittivity, which can be accounted for by the higher permittivity of larger particles.

The microwave permittivity and absorption data for samples differing in the concentration of nanoparticles are presented in Figs. 11 and 12. These data can be used to evaluate the amplitudes and time constants of relaxation processes. For samples 1 and 2, the reduction in permittivity, with no significant changes in losses in the working frequency range, can be accounted for by a reduction in relaxation rate without changes in relaxation time. Increasing the nanoparticle content to 20 wt % (sample 3) reduces the relaxation time, with no marked changes in relaxation rate. Note that increasing the nanoparticle content of the polymer tends to reduce the relaxation time and raise the relaxation rate. These relationships, as well as the low-frequency data, can be understood in terms of the polarization of the metal-containing nanoparticles, whose permittivity increases with particle size. The present results demonstrate that the microwave absorption and permittivity of our samples vary little in a broad frequency range.

Samples 1–5 were characterized by magnetic resonance measurements. The spectrometer recorded the derivative of microwave absorption with respect to external field H_0. The measurements were performed at room temperature using samples in the form of thin

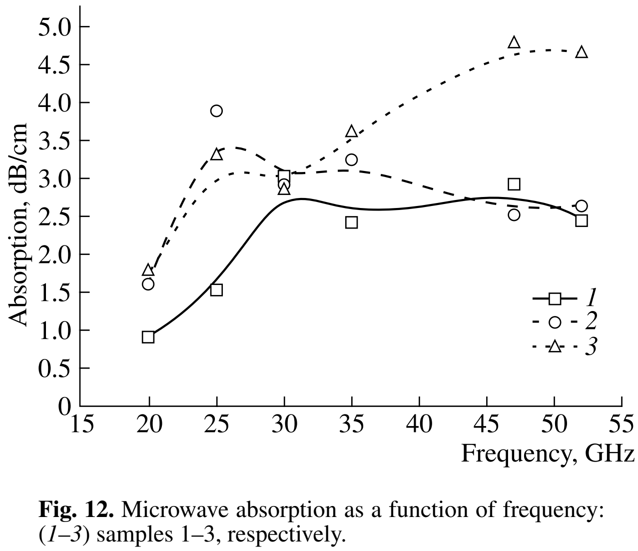

Fig. 12. Microwave absorption as a function of frequency: (*1–3*) samples 1–3, respectively.

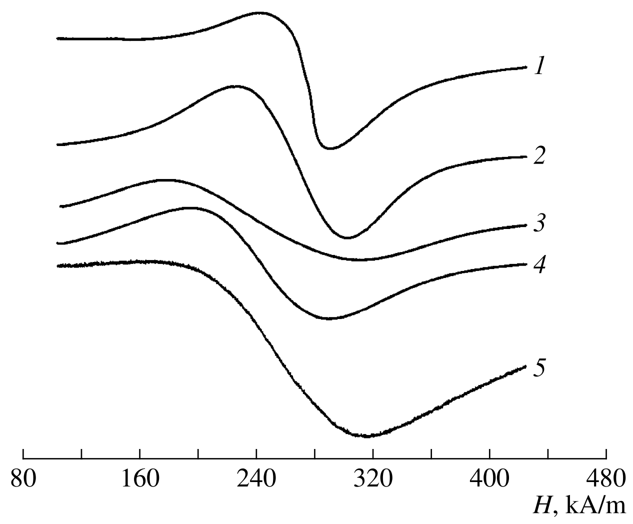

Fig. 13. Room-temperature magnetic resonance spectra: (*1–5*) samples 1–5, respectively.

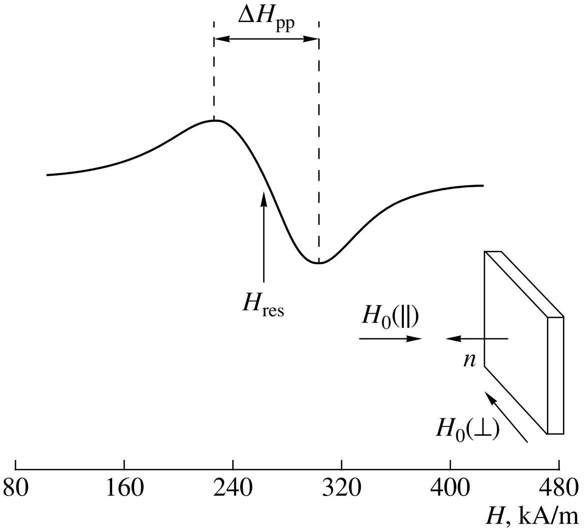

Fig. 14. Geometry of EMR measurements: ΔH_{pp} is the linewidth, H_{res} is the resonance field, H_0 is the external magnetic field, and *n* is the normal to the sample surface.

(0.5- to 1-mm in thickness) square (2- to 3-mm side) plates. The spectra of all the samples show inhomogeneously broadened singlets (Fig. 13). To analyze the spectra, we determined the linewidth ΔH_{pp} and resonance field H_{res} for two field directions: parallel (||) and perpendicular (⊥) to the sample surface (Fig. 14). The values of ΔH_{pp}, $H_{res}(\perp)$, and $H_{res}(\perp) - H_{res}(||)$ are listed in Table 4.

In samples 1–4, the EMR linewidth increases with metal content (Fig. 13), characteristic of ferromagnetic nanoparticles. ΔH_{pp} increases most rapidly upon an increase in metal content from 10 to 20% (samples 2 and 3, respectively). This fits well with the conclusion that sample 3 has a reduced relaxation time, inferred from permittivity and microwave absorption data. The EMR linewidth, however, depends not only on the total metal concentration but also on the average nanoparticles size. In particular, the smaller particle size in sample 4 compared to sample 3 (2.4 and 11.5 nm, respectively) leads to significant narrowing of the resonance, by more than 30% (Table 4).

The largest linewidth was observed in sample 5, containing cobalt nanoparticles. This may be due to a significant magnetization of the sample and scatter of local magnetic fields. The scatter may arise from the presence of different phases in the cobalt nanoparticles (cobalt metal and cobalt oxides), differing in magnetic properties. The magnetization of the samples was estimated from the difference in resonance magnetic field between two sample orientations, which is due to the difference in the corresponding demagnetizing factors. In a field normal to the plate surface, the demagnetizing factor is rather large (4π in an infinite plate). In a field parallel to the plate surface, it is close to zero. It can be seen from Table 4 that the magnetization of the sample containing cobalt nanoparticles is several times higher than that of the sample containing magnetite nanoparticles in the same concentration (20%) and of nearly the same size.

Table 4. EMR parameters of samples 1–5

Sample no.	ΔH_{pp}, kA/m	$H_{res}(\perp)$, kA/m	$H_{res}(\perp) - H_{res}(\|\|)$, kA/m
1	48.54	250.57	0.0
2	76.40	266.60	3.98
3	132.90	246.70	3.98
4	94.70	246.70	3.18
5	141.65	250.68	11.14

We also studied the low-field microwave absorption hysteresis, which characterizes the remanent magnetic moment of the material. The highest remanent magnetization (~100 to 200 G) was observed at the highest nanoparticle concentration. All the above demonstrates that, among the materials containing magnetite and cobalt nanoparticles, the highest magnetization (including the remanent one) is offered by the cobalt-containing samples and that, on the whole, increasing the metal concentration improves the magnetic properties of the nanomaterials.

CONCLUSIONS

We prepared nanocomposites consisting of narrowly sized metal-containing nanoparticles embedded in a polyethylene matrix and established conditions for the fabrication of thick films and bulk materials from the resulting polymer powders.

Our results on the electrical properties of the polyethylene-matrix nanocomposites containing iron nanoparticles demonstrate that, with increasing nanoparticle concentration in the polymer matrix, the dielectric permittivity and absorption coefficient of the nanostructured materials increase.

The electrical properties (dielectric permittivity and resistivity) of the composites depend on the nanoparticle size and concentration.

Our results demonstrate that the microwave absorption and permittivity of the nanocomposites vary little in a broad frequency range.

The magnetization (including the remanent one) of the cobalt-containing nanomaterials is higher than that of the iron-containing samples. In addition, the magnetic properties of the synthesized nanomaterials depend on the concentration of metal-containing nanoparticles.

ACKNOWLEDGMENTS

This work was supported by the Russian Foundation for Basic Research (grant nos. 07-03-00885, 07-08-00523, 06-03-72031-MNTI, and 05-03-32083), the President's Grants Council (grant no MK-253.2007.3), the National Science Promotion Foundation, INTAS (grant no. 05-1000008-7834), the International Science and Technology Center (grant no. 3457), and the Russian Academy of Sciences (basic research programs *Development of Chemical Processes and Creation of Novel Materials* and *Development of Effective Approaches to Chemical Analysis and Structural Characterization of Substances and Materials*).

REFERENCES

1. Pomogailo, A.D., Rozenberg, A.S., and Uflyand, I.E., *Nanochastitsy metallov v polimerakh* (Metal Nanoparticles in Polymers), Moscow: Khimiya, 2000.
2. Gubin, S.P., Koksharov, Yu.A., Khomutov, G.B., and Yurkov, G.Yu., Magnetic Nanoparticles: Preparation, Structure, and Properties, *Usp. Khim.*, 2005, vol. 74, no. 6, pp. 539–574.
3. Gubin, S.P., Yurkov, G.Yu., and Kosobudsky, I.D., Nanomaterials Based on Metal-Containing Nanoparticles in Polyethylene and Other Carbon-Chain Polymers, *Int. J. Mater. Prod. Technol.*, 2005, vol. 23, nos. 1–2, pp. 2–25.
4. Scomski, R., Nanomagnetics, *J. Phys.: Condens Matter*, 2003, vol. 15, pp. R841–R896.
5. Hyeon, T., Chemical Synthesis of Magnetic Nanoparticles, *Chem. Commun.*, 2003, pp. 927–934.
6. Lin, X.-M. and Samia, A.C.S., Synthesis, Assembly, and Physical Properties of Magnetic Nanoparticles, *J. Magn. Magn. Mater.*, 2006, vol. 305, pp. 100–109.
7. Kosobudsky, I.D. and Gubin, S.P., Metallic Clusters in Polymer Matrices: A New Type of Metal-Filled Polymers, *Vysokomol. Soedin.*, 1985, vol. 27, no. 3, pp. 689–695.
8. Smith, T.W. and Wychick, D., Colloidal Iron Dispersions Prepared via the Polymer-Catalyzed Decomposition of Iron Pentacarbonyl, *J. Phys. Chem.,* 1980, vol. 84, no. 12, pp. 1621–1629.
9. Gubin, S.P., What is a Nanoparticle? Current Trends in the Development of Nanochemistry and Nanotechnology, *Ross. Khim. Zh.,* 2000, vol. 44, no. 6, pp. 23–31.
10. Zanetti, M. and Costa, L., Preparation and Combustion Behaviour of Polymer/Layered Silicate Nanocomposites Based upon PE and EVA, *Polymer,* 2004, vol. 45, pp. 4367–4373.
11. Zanetti, M., Camino, G., Reichert, P., and Mülhaupt, R., Thermal Behaviour of Poly(propylene) Layered Silicate Nanocomposites, *Macromol. Rapid Commun.*, 2001, vol. 22, no. 3, pp. 176–180.
12. Korobov, M.S., Yurkov, G.Yu., Kozinkin, A.V., et al., Metal-Containing Poly(tetrafluoroethylene): A Novel Material, *Neorg. Mater.*, 2004, vol. 40, no. 1, pp. 31–40 [*Inorg. Mater.* (Engl. Transl.), vol. 40, no. 1, pp. 26–34].
13. Yurkov, G.Yu., Baranov, D.A., Dotsenko, I.P., and Gubin, S.P., New Magnetic Materials Based on Cobalt and Iron-Containing Nanoparticles, *Composites,* 2006, vol. 37, no. 6, pp. 413–417.
14. Zanetti, M., Lomakina, S., and Camino, G., Polymer Layered Silicate Nanocomposites, *Macromol. Mater. Eng.*, 2000, vol. 279, pp. 1–9.
15. Xia, X., Cai, S., and Xie, C., Preparation, Structure, and Thermal Stability of Cu/LDPE Nanocomposites, *Mater. Chem. Phys.*, 2006, vol. 95, pp. 122–129.
16. Hong, J.I., Schadler, L.S., and Siegel, R.W., Rescaled Electrical Properties of ZnO/Low Density Polyethylene Nanocomposites, *Appl. Phys. Lett.*, 2003, vol. 82, no. 12, pp. 1956–1958.
17. Brosseau, C., Quéffélec, P., and Talbot, P., Microwave Characterization of Filled Polymers, *J. Appl. Phys.*, 2001, vol. 89, no. 8, pp. 4532–4540.
18. Ng, C.B., Ash, B.J., Schadler, L.S., and Siegel, R.W., A Study of the Mechanical and Permeability Properties of Nano- and Micron-TiO_2 Filled Epoxy Composites, *Adv. Compos. Lett.*, 2001, vol. 10, no. 3, pp. 101–111.
19. Chung, K.T., Sabo, A., and Pica, A.P., Electrical Permittivity and Conductivity of Carbon Black–Polyvinyl Chloride Composites, *J. Appl. Phys.*, 1982, vol. 53, no. 10, pp. 6867–6879.
20. Zhang, X.W., Pan, Y., Zheng, Q., et al., Time Dependence of Piezoresistance for the Conductor-Filled Polymer Composites, *J. Polym. Sci., Part B: Polym. Phys.*, 2000, vol. 38, no. 21, pp. 2739–2749.
21. Hong, J.I., Winberg, P., Schadler, L.S., and Siegel, R.W., Dielectric Properties of Zinc Oxide/Low Density Polyethylene Nanocomposites, *Mater. Lett.*, 2005, vol. 59, no. 4, pp. 473–476.
22. Cadek, M., Coleman, J.N., Barron, V., et al., Morphological and Mechanical Properties of Carbon-Nanotube-Reinforced Semicrystalline and Amorphous Polymer Composites, *Appl. Phys. Lett.*, 2002, vol. 81, no. 27, pp. 5123–5125.
23. Du, F., Scogna, R.C., Zhou, W., et al., Nanotube Networks in Polymer Nanocomposites: Rheology and Electrical Conductivity, *Macromolecules*, 2004, vol. 37, no. 24, pp. 9048–9055.

24. Hill, D.E., Lin, Y., Rao, A.M., et al., Functionalization of Carbon Nanotubes with Polystyrene, *Macromolecules*, 2002, vol. 35, no. 25, pp. 9466–9471.

25. Dang, Z.-M., Zhang, Y.-H., and Tjong, S.-C., Dependence of Dielectric Behavior on the Physical Property of Fillers in the Polymer-Matrix Composites, *Synth. Met.*, 2004, vol. 146, no. 1, pp. 79–84.

26. Zois, H., Mamunya, Y.P., and Apekis, L., Structure and Dielectric Properties of a Thermoplastic Blend Containing Dispersed Metal, *Macromol. Symp.*, 2003, vol. 198, no. 1, pp. 461–472.

27. Dang, Z., Fan, L., Zhao, S., and Nan, C., Dielectric Properties and Morphologies of Composites Filled with Whisker and Nanosized Zinc Oxide, *Mater. Res. Bull.*, 2003, vol. 38, no. 3, pp. 499–507.

28. Gangopadhyay, R. and De, A., Conducting Polymer Nanocomposites: A Brief Overview, *Chem. Mater.*, 2000, vol. 12, no. 3, pp. 608–622.

29. Sumita, M., Sakata, K., Asai, S., et al., Dispersion of Fillers and the Electrical Conductivity of Polymer Blends Filled with Carbon Black, *Polym. Bull.*, 1991, vol. 25, no. 2, pp. 265–271.

30. Flandin, L., Verdier, M., Boutherin, B., et al., A 3-D Numerical Simulation of AC Electrical Properties of Short Fiber Composites, *J. Polym. Sci., Part B: Polym. Phys.*, 1999, vol. 37, no. 8, pp. 805–814.

31. Kawasumi, M., Hasegawa, N., Kato, M., et al., Preparation and Mechanical Properties of Polypropylene–Clay Hybrids, *Macromolecules*, 1997, vol. 30, no. 20, pp. 6333–6338.

32. Wang, Y. and Herron, N., Nanometer-Sized Semiconductor Clusters: Materials Synthesis, Quantum Size Effects, and Photophysical Properties, *J. Phys. Chem.,* 1991, vol. 95, no. 2, pp. 525–532.

33. Siegel, R.W., Nanostructured Materials-Mind over Matter, *Nanostruct. Mater.*, 1993, vol. 3, nos. 1–6, pp. 1–18.

34. Gleiter, H., Weissmuller, J., Wollersheim, O., and Wurschum, R., Nanocrystalline Materials: A Way to Solids with Tunable Electronic Structures and Properties, *Acta Mater.*, 2001, vol. 49, no. 4, pp. 737–745.

35. Gubin, S.P., Spichkin, Yu.I., Koksharov, Yu.A., et al., Magnetic and Structural Properties of Co Nanoparticles in Polymeric Matrix, *J. Magn. Magn. Mater.*, 2003, vol. 265, no. 2, pp. 234–242.

36. Li, X.H., Tjong, S.C., Meng, Y.Z., et al., Fabrication and Properties of Poly(propylene carbonate)/Calcium Carbonate Composites, *J. Polym. Sci., Part B: Polym. Phys.*, 2003, vol. 41, no. 154, pp. 1806–1813.

37. Tjong, S.C. and Meng, Y.Z., Structural–Mechanical Relationship of Epoxy Compatibilized Polyamide 6/Polycarbonate Blends, *Mater. Res. Bull.*, 2004, vol. 39, no. 11, pp. 1791–1801.

38. Tjong, S.C. and Bao, S.P., Preparation and Nonisothermal Crystallization Behavior of Polyamide 6/Montmorillonite Nanocomposites, *J. Polym. Sci., Part B: Polym. Phys.*, 2004, vol. 42, no. 15, pp. 2878–2891.

39. Von Hippel, A.R., *Dielectric Materials and Applications,* New York: The Technology Press of MIT and John Wiley and Sons, 1954.

40. Brandt, A.A., *Issledovanie dielektrikov na sverkhvysokikh chastotakh* (Microwave Characterization of Dielectrics), Moscow: Fizmatgiz, 1963.

41. Kozinkin, A.V., Vlasenko, V.G., Gubin, S.P., et al., Clusters in a Polymer Matrix: II. Investigation of the Composition and Structure of Iron-Containing Clusters in a Polyethylene Matrix, *Neorg. Mater.,* 1996, vol. 32, no. 4, pp. 422–428 [*Inorg. Mater.* (Engl. Transl.), vol. 32, no. 4, pp. 376–381].

42. Yurkov, G.Yu., Popkov, O.V., Koksharov, Yu.A., et al. Fe-Containing Nanoparticles on the Surface of Silica Microgranules, *Neorg. Mater.*, 2006, vol. 42, no. 8, pp. 970–975 [*Inorg. Mater.* (Engl. Transl.), vol. 42, no. 8, pp. 877–882].

43. Yurkov, G.Yu., Baranov, D.A., Kozinkin, A.V., et al., Cobalt-Containing Core–Shell Nanoparticles on the Surface of Poly(tetrafluoroethylene) Microgranules, *Neorg. Mater.*, 2006, vol. 42, no. 9, pp. 1112–1119 [*Inorg. Mater.* (Engl. Transl.), vol. 42, no. 9, pp. 1012–1019].

44. Gubin, S.P., Yurkov, G.Yu., Korobov, M.S., et al., Immobilization of Metallcontaining Nanoparticles on the Surface of Polytetrafluoroethylene Nanogranules, *Acta Mater.*, 2005, vol. 53, no. 5, pp. 1407–1413.